Surveying young stars with Gaia: Orion and the Solar neighbourhood

Zari, E.M.

5

Searching for runaway stars in Gaia DR2

We search for early type runaway stars within 1 kpc from the Sun by using the data of the second data release of the *Gaia* satellite (*Gaia* DR2) and the stellar parameters provided in the `StarHorse` catalogue. We select upper main sequence (UMS) sources by applying simple photometric cuts. Our sample consists of O-, B- and early A-type sources. We study the tangential velocity, and, when possible, the total velocity distribution of our sample, and we classify as candidate runaway stars those sources that have tangential velocities significantly different from the rest of the population (2σ) or total velocities higher than $30\,\mathrm{km\,s^{-1}}$. We study the orbits of the candidate runaway stars with literature radial velocities, and we find that around half of our candidates originated from beyond 1 kpc. We focus on the runaway star candidates in the Orion and Scorpius-Centaurus (Sco-Cen) regions. In Orion, we confirm previously known runaway stars and we enlarge the sample by adding 6 new runaway candidates. In Sco-Cen we identify two runaway star candidates that likely share the same origin. Finally, we discuss our findings in the context of other studies, and we estimate the completeness of our sample. More radial velocities are needed to obtain a more complete sample.

Based on:
E. Zari, T. Marchetti,
A.G.A. Brown, P.T. de Zeeuw
to be submitted to A&A

5.1 Introduction

O and B-type stars are often found in isolated locations, and do not appear to be members of clusters or associations. A large fraction of them moves at very high velocities: these are referred to as "runaway" stars (Blaauw 1952; Ambartsumian 1955; Hoogerwerf et al. 2001). The typical velocity threshold adopted to define a runaway star is $v > 30\,\mathrm{km\,s^{-1}}$ (Blaauw 1956; Gies & Bolton 1986; De Donder et al. 1997; Hoogerwerf et al. 2001; Dray et al. 2005; Eldridge et al. 2011), although sometimes $v > 40\,\mathrm{km\,s^{-1}}$ is used (Blaauw 1961; de Wit et al. 2005; Boubert & Evans 2018). Contrary to the majority of young, un-evolved massive stars, runaway stars present an almost complete absence of multiplicity (Chini et al. 2012; Sana et al. 2012; Almeida et al. 2017). Further, they show large rotational velocities and enhanced helium surface abundances (Hoogerwerf et al. 2001).

Two main mechanisms have been suggested to explain the origin of runaway stars: the binary supernova scenario (BSS) and the dynamical ejection scenario (DES).

According to the BSS (Blaauw 1961; Zwicky 1957; Boersma 1961), a runaway star receives its velocity when the primary component of the massive binary system explodes as a supernova. What remains of the binary after the explosion is a compact object, which, depending on the details of the preceding binary evolution, the eccentricity of the orbit, and the kick velocity due to the asymmetry of the supernova explosion, might or not remain bound to the runaway star (Renzo et al. 2019b).

In the DES (Poveda et al. 1967; Leonard 1991), runaways are formed through gravitational interactions between stars in dense, compact clusters. DES runaways have the following characteristics: 1) they are formed in high density environments, i.e. in young open clusters; 2) they do not show signs of binary evolution; 3) they are expected to be mostly single stars.

Which of the two formation mechanisms is mostly responsible for runaway stars is still unclear. The relative importance of the two scenarios has been investigated by studying the statistical properties of the ensemble of runaway stars or by focusing on individual runaways in detail.

By analysing a sample of 56 nearby runaway stars and 9 radio pulsars, Hoogerwerf et al. (2001) estimated that the disruption of binaries is responsible for roughly two thirds of observed runaways, however this claim could not be confirmed in the reanalysis of the same sample by Jilinski et al. (2010). Boubert et al. (2017) searched for runaways from the progenitors of nearby Galactic core-collapse supernova remnants (SNRs) by using the first data release of the *Gaia* satellite (*Gaia* DR1) and found likely companions for four SNRs. Tetzlaff et al. (2011) select young (age $<$ 50 Myr) stars of any spectral type in the Hipparcos catalogue, and identify those with large peculiar velocities, finding in total 2547 candidate runaway stars. Boubert & Evans (2018) measured the fraction of runaway B-type emission-line stars (Be stars), and conclude that all Be stars could be explained by an origin in mass-transfer binaries. Maíz Apellániz & Weiler (2018) detected runaway stars by using *Gaia* DR1 proper motions, and suggest that the majority of them is produced by supernova explosions. Renzo et al. (2019a) investigated the kinematics of VFTS682, located in 30 Doradus (in the Large Magellanic Cloud), by combining the second *Gaia* data release (*Gaia* DR2) and *Hubble Space Telescope* data, and conclude that if was ejected from the central cluster.

Theoretical and numerical studies have focused on deriving analytic relations to iden-

tify dynamically formed runaway stars (Ryu et al. 2017), and predicting the peculiar velocities that massive binary systems obtain when the primary star collapses and disrupts the system, and investigating which physical processes leave a clear imprint and may therefore be constrained observationally (Renzo et al. 2019b). Renzo et al. (2019b) find in particular that the majority of the systems ejects a star at velocity below 30 $\mathrm{km\,s^{-1}}$, i.e., a walkaway star (de Mink et al. 2012), and that runaways resulting from the disruption of binaries rarely exceed 60 $\mathrm{km\,s^{-1}}$.
In this study we search for Upper Main Sequence (UMS) runaway stars within 1 kpc by using the `StarHorse` catalogue (Anders et al. 2019), which is based on the combination of *Gaia* DR2 with other photometric catalogues (PanSTARRS-1, 2MASS, and AllWISE). Our goal is to construct a catalogue of fast moving sources in the (extended) solar neighbourhood and to analyse their statistical properties. The data used are presented in Section 5.2, where we describe the quality flags applied and the UMS selection criteria. In Section 5.3 we describe the methods used to identify the runaway candidates and to study their orbits. In Section 5.4 we present our results, which are discussed in Section 5.5. Conclusions are drawn in Section 5.6.

5.2 Data

To create the `StarHorse` catalogue, Anders et al. (2019) combine parallaxes and optical photometry from *Gaia* DR2 with the photometric catalogues PanSTARRS-1, 2MASS, and AllWISE, and employ a Bayesian approach to derive stellar parameters, distances and extinction for *Gaia* DR2 sources brighter than $G = 18\,\mathrm{mag}$. `StarHorse` does not contain all the *Gaia* DR2 sources, since the stars for which the code did not converge are not reported in the catalogue. This usually occurs for objects which cannot be fitted onto the model grid within the extinction limits used in the paper (e.g. highly reddened stars, F. Anders, private communication). The draw-back of this approach is that the sample is not complete, and most importantly, that estimating our incompleteness level is not trivial (see Section 5.5). However, we decided to use `StarHorse` to take properly into account extinction and reddening, as our selection of early type stars is strongly based on their position in the colour-magnitude diagram.
We consider stars nominally closer than 1 kpc ($\varpi > 1\,\mathrm{mas}$), and we select them by applying the conditions `SH_OUTFLAG` = "00000" and `SH_GAIAFLAG` = "000", as recommended by Anders et al. (2019). The three digits of `SH_GAIAFLAG` correspond to:

- *Re-normalized unit weight error* (*RUWE*) *flag* (see Lindegren et al. 2018, Appendix C for the definition of the unit weight error and the web-page:`https://www.cosmos.esa.int/web/gaia/dr2-known-issues` for the definition of the RUWE). The first digit corresponds to 0 if the RUWE < 1.4.
- *Colour excess factor flag*. It corresponds to 0 if Eq. C.2 in (Lindegren et al. 2018) is satisfied.
- *Variability flag*. It corresponds to the *Gaia* DR2 `phot_variable_flag`.

The five digits of `SH_OUTFLAG` correspond to:

- *Main* `StarHorse` *reliability flag*: it is equal to 1 when the distance posterior probability is very broad (see Anders et al. 2019, for the definition of "broad").

- *Large distance flag*: for some stars `StarHorse` delivers very large distances, many of which are affected by significant biases. The second digit equal to 0 corresponds to median posterior distance smaller than 20 kpc.
- *Unreliable extinction flag*: it is set to 0 to exclude stars with significantly negative extinctions, or A_V values close to the prior boundary at $A_V = 4$.
- *Large A_V uncertainty flag*: it is set to 0 to exclude stars with very large uncertainty on A_V, probably due to uncertain or incomplete input data.
- *Very small uncertainty flag*: it indicates that the posterior uncertainty on distance, or extinction, or temperature, or $\log g$, or mass is small and most likely underestimated. By setting the fifth digit to 0, stars with unrealistic uncertainties are excluded.

In the following, we use the `StarHorse` parameter `dist50`, which corresponds to the median of the distance posterior distribution, as the distance to a star, and we call it d for brevity. The `StarHorse` distances are derived by taking into account different parallax offsets, which depend on the source G-magnitude, and by re-scaling the parallax errors following a slightly modified version of the re-calibration proposed in Lindegren et al. (2018).
Similarly to Zari et al. (2018), we select Upper Main Sequence (UMS) stars by using the following conditions:

$$\begin{aligned} M_{G,0} &\leqslant 0\,\mathrm{mag}; \\ (G_{\mathrm{BP}} - G_{\mathrm{RP}})_0 &\leqslant 0.5\,\mathrm{mag}, \end{aligned} \tag{5.1}$$

where M_G is the absolute magnitude in the *Gaia* G band, and $(G_{\mathrm{BP}} - G_{\mathrm{RP}})$ is the colour in the *Gaia* G_{BP} and G_{RP} bands. The de-reddened absolute magnitude and colour $M_{G,0} = M_G - A_G$ and $(G_{\mathrm{BP}} - G_{\mathrm{RP}})_0 = G_{\mathrm{BP}} - G_{\mathrm{RP}} - E(BP - RP)$ are provided in the `StarHorse` catalogue. [1] The sample consists of 17408 sources. By cross-matching with Simbad we find that ∼80% of them has a measured spectral type. Most of the sources are B-type stars (7684, i.e. 44%), 5993 (34%) stars are early A-type stars, and only 40 sources are O-type stars.
To select UMS candidate runaway stars we rely primarily on their tangential velocity. To trace back their orbits in 3D space radial velocities are however needed. We therefore cross-match our sample with external radial velocity catalogues, in particular: the XHIP catalogue (3088 sources, Anderson & Francis 2012, and references therein) and RAVE DR5 (254 sources, Kunder et al. 2017).

5.3 Method

We first select as candidate runways stars those whose tangential velocity is significantly different from the rest of the population (Section 5.3.1). At this stage we do not consider radial velocities because the majority of the stars selected in Section 5.2 does not have a measured radial velocity. This however results in a loss of completeness, as we neglect sources with high radial velocity but tangential velocity comparable to the

[1] The column names are: `mg0` and `bprp0` respectively.

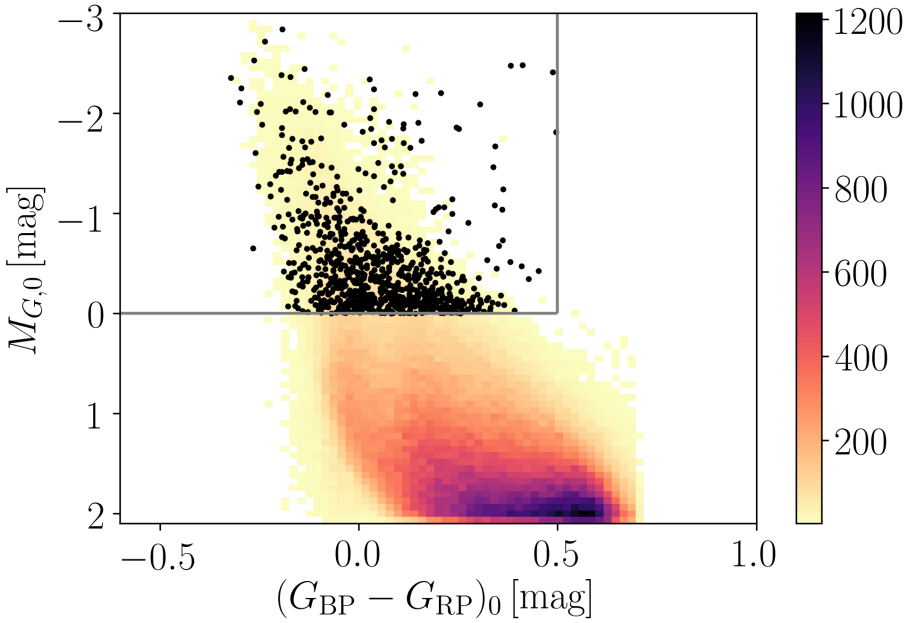

Figure 5.1: Colour-magnitude diagram corrected for extinction and reddening of the sources selected by applying the conditions `SH_OUTFLAG = "00000"` and `SH_GAIAFLAG = "000"`. They grey lines correspond to $M_{\rm G,0} = 0\,$mag and $G_{\rm BP} - G_{\rm RP} = 0\,$mag. The black dots represent the candidate runaway stars selected in Section 3.1.

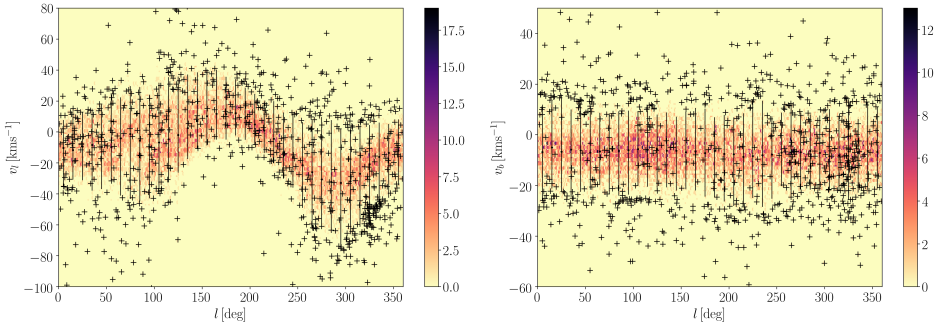

Figure 5.2: The 2D histogram represent the tangential velocity along longitude (v_l, left) and latitude (v_b, right) as a function of longitude for the UMS sample. The black crosses represent the candidate runaway stars selected in Sec. 5.3.1. The vertical bars represent the 16th and 84th percentiles of the v_l and v_b distributions at each longitude bin.

reflex solar motion. Therefore, in Section 5.3.2 we consider the sources with measured radial velocity, we estimate the peculiar total velocity v_{tot}, and we include as candidate runaway stars the sources with total peculiar velocity $v_{tot} > 30\,\mathrm{km\,s^{-1}}$ which were not already selected in Section 5.3.1. In this way we obtain 1197 candidate runaway stars, of which 385 are classified as O- and B- type stars (although there are only 4 O-type stars), and 223 do not have any spectral type from literature. The rest of the sources is of spectral type A or later. We will focus the rest of our analysis (in particular the orbit integration) on the O and B-type stars with measured radial velocities. We include the sources with spectral type A, the sources without a spectral type from literature, and the sources without radial velocities (of any spectral type) in the catalogue which will accompany the paper, but we will not analyse those sources further in this study. Finally, to understand the origin of our runaway candidates, and to determine whether their ejection location was within 1 kpc from the Sun, we perform a three-dimensional (3D) trace back in a galactic potential by integrating our candidate orbits back in time (5.3.3).

5.3.1 Selection of sources with high tangential velocity

Fig. 5.2 shows the tangential velocity in the longitude and latitude direction (v_l and v_b) vs. longitude for the stars selected in Section 2; v_l and v_b are defined as:

$$\begin{aligned} v_l &= A\,\mu_{l^*}/\varpi, \\ v_b &= A\,\mu_b/\varpi, \end{aligned} \tag{5.2}$$

where $A = 4.74047\mathrm{km\,s^{-1}\,yr}$. To select our candidates, we define the quantity:

$$\Delta = \sqrt{\left(\frac{v_l - \bar{v}_l}{\sigma_l}\right)^2 + \left(\frac{v_b - \bar{v}_b}{\sigma_b}\right)^2} \tag{5.3}$$

and

$$\sigma_{l,b} = \frac{v_{l,b,16} - v_{l,b,84}}{2}, \tag{5.4}$$

where $\bar{v}_{l,b}$, $v_{l,b,16}$, and $v_{l,b,84}$ are the 50th, 16th and 84th percentiles of the tangential velocities per longitude bin. The quantities $v_{l,pec} = v_l - \bar{v}_l$ and $v_{b,pec} = v_b - \bar{v}_b$ correspond to the peculiar velocity along l and b. We select stars with $\Delta > 3.$, which corresponds roughly to the 95th percentile of the Δ distribution. With this criterion we select stars with tangential velocities strongly deviating from the mean tangential motion as a function of longitude angle. The mean tangential velocity mainly reflects the projection of the solar motion in the different directions on the sky and also to differential galactic rotation. The sample consist of 857 sources, which corresponds to the 5% of the sources selected in Section 5.2. Fig. 5.3 (left) shows the reduced tangential velocity distribution of the stars selected through the Δ condition (orange histogram) and of all the stars in our sample (grey histogram). Both histograms are normalised. The minimum reduced tangential velocity is $\approx 17\,\mathrm{km\,s^{-1}}$, while the peak of the distribution is at $v_t \approx 41\,\mathrm{km\,s^{-1}}$.

5.3.2 Selection of sources with high total velocity

25% of the sources selected in Section 5.2 have literature radial velocities, and 300 of those are selected as runaway stars (35%) only based on their tangential velocity. Fig. 5.4 shows the radial velocity v_r as a function of l for our UMS sample (gray dots), and for our candidate runaway stars (blue crosses). The orange dots correspond to the median radial velocity per latitude bin. Similarly to Fig. 5.2, the sinusoidal trend visible in Fig. 5.4 reflects the solar motion. Many sources that have a high radial velocity compared to the solar motion are not selected as candidate runaway stars by considering the tangential velocity only. Following Hoogerwerf et al. (2001) we therefore select stars whose total peculiar velocity is larger than $30\,\mathrm{km\,s^{-1}}$, where the radial peculiar velocity is defined as $v_{r,pec} = v_r - \bar{v}_r$, and $\bar{v}_r$ is the mean radial velocity per latitude bin and the total peculiar velocity is: $v_{tot,pec} = \sqrt{v_{r,pec}^2 + v_{l,pec}^2 + v_{b,pec}^2}$. In this way we add 341 sources to those selected by using only the proper motions. This brings the total number of runaway candidates to 1197 sources. Fig. 5.3 shows the total peculiar velocity distribution of our sample (light grey histogram), and the total peculiar velocity distribution of the runaway star candidates (blue histogram).

Fig. 5.5 shows the sky distribution of UMS sources selected by applying Eq. 5.1 (grey dots, top) and the distribution of candidate runaway stars (black dots, bottom). UMS stars are located in the galactic plane, and their dispersion along the Z-axis (where Z is the third component of the vector (X, Y, Z), indicating the position of a star in Cartesian galactic coordinates) is around 200 pc.

5.3.3 3D trace back

To derive the birthplace of the candidate runaway stars, we perform an orbit integration using the python package `gala` (Price-Whelan 2017). We use the `gala` *Milky Way Potential*, which consist of a spherical nucleus and bulge, a Miyamoto-Nagai disk, and a spherical NFW dark matter halo. We define the Sun's velocity (in Galactic coordinates) as $(U, V, W)_\odot = (11.1, 12.24, 7.25)\,\mathrm{km\,s^{-1}}$ following Schönrich (2012). The circular rotation velocity at the Sun position is $V_{circ} = 238\,\mathrm{kms^{-1}}$, and the Sun's height with respect to the Galactic plane is 25 pc (Bland-Hawthorn & Gerhard 2016).

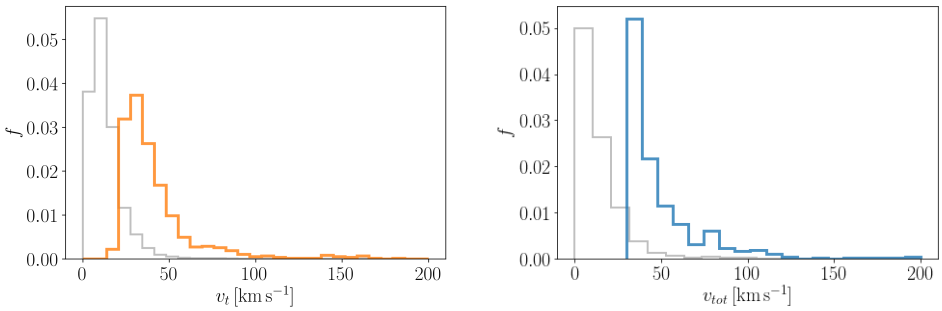

Figure 5.3: Left: Normalised histograms of the reduced total tangential velocity for all the stars selected (grey histogram) and for the star following the condition $\Delta > 3$ (orange histogram). The minimum of the candidate runaway tangential velocity distribution is around $17\,\mathrm{km\,s^{-1}}$, the maximum is around $164\,\mathrm{km\,s^{-1}}$ and the mean $\sim 41\,\mathrm{km\,s^{-1}}$. Right:Normalised histograms of the reduced total velocity for all the stars with radial velocity (lgrey histogram), and for the sources with reduced total velocity higher than 30 $\mathrm{km\,s^{-1}}$ (blue histogram).

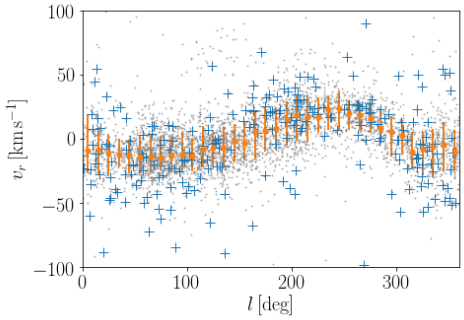

Figure 5.4: Radial velocity versus galactic longitude for the stars selected by applying the conditions `SH_OUTFLAG = "00000"` and `SH_GAIAFLAG = "000"`. The blue crosses represent the candidate runaway stars selected in Section 3.1. The orange dots correspond to the median radial velocity values per latitude bin, and the error bars the 16th and 84th percentile respectively.

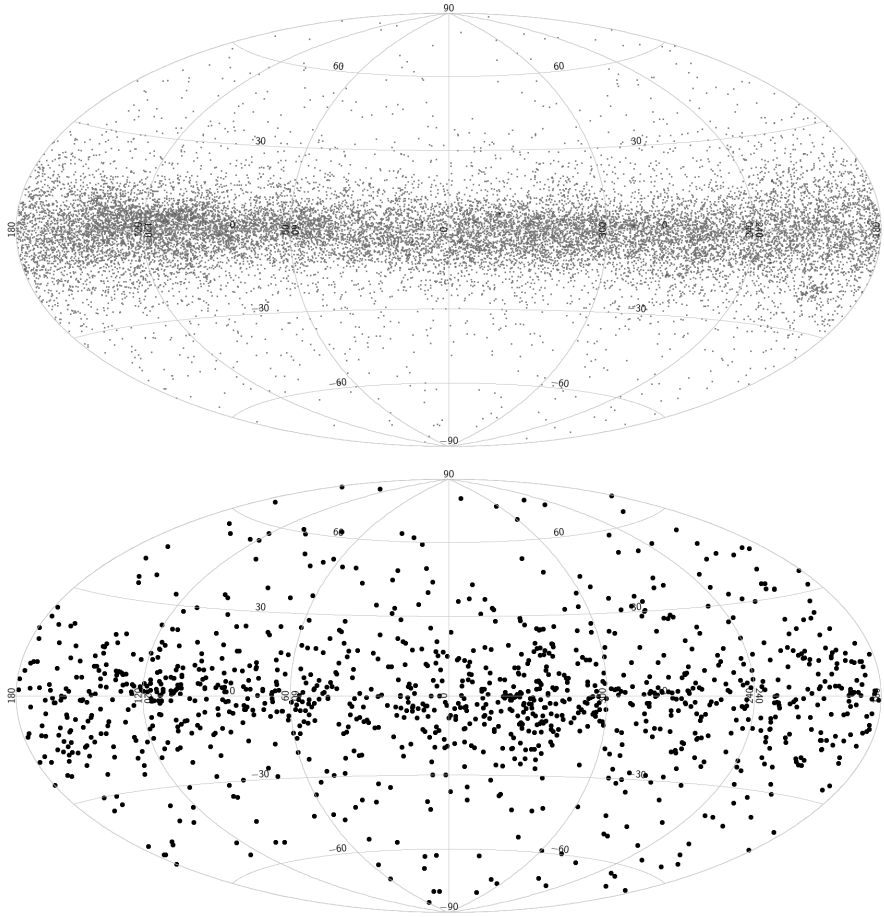

Figure 5.5: Top: distribution in the sky of the sources selected with Eq. 1. Bottom: distribution of the candidate runaway stars selected in Section 3.1 and 3.2. The distribution of UMS sources peaks towards the Galactic Plane, as well as the distribution of runaway candidates.

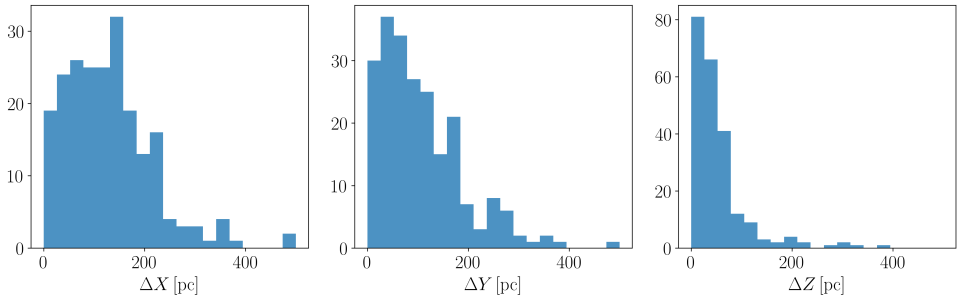

Figure 5.6: Histograms showing the quantities $(X, Y, Z)_{50} - (X, Y, Z)_{16}$ (left, centre, right respectively) at $t = -10$ Myr. Th distributions indicate the uncertainty in the trace-back of the candidate runaway stars. The median of the distributions are: $\approx$ 123, 89, and 38 pc respectively.

The trace back consists of two steps. We first perform a trace back with a long integration time ($t = 100$Myr) and with a large time step $\delta\, t = 0.5\,\mathrm{Myr}$ to estimate which candidate runaway stars originate from the solar neighbourhood ($d < 1$ kpc). A star with a velocity of $30\,\mathrm{km\,s^{-1}}$ travels $\sim$ 1 kpc in 33 Myr, however we chose a longer trace-back time to account for the possibility of the ejection taking place at distances much farther than 1 kpc. For stars with $|Z_0| > 0.2\,\mathrm{kpc}$ (the suffix 0 indicates the current position of the star), we compute the "ejection distance" as the distance at the time when the star enters the disc, which we define as the slab with $|Z| < 0.2\,\mathrm{kpc}$. The value $|Z| = 0.2\,\mathrm{kpc}$ corresponds to the dispersion along the Z axis of the stars selected in Section 5.2. For stars with $|Z_0| < 0.2\,\mathrm{kpc}$, i.e. stars that are already in the disc, we define the ejection distance as the distance when the star first crosses the plane $Z = 0\,\mathrm{kpc}$.

We repeat the trace back for a shorter time and a smaller time step ($t = 10\,\mathrm{Myr}$ and $\delta\, t = 0.1\,\mathrm{Myr}$) to precisely derive the birth place of the stars ejected within $d < 1\,\mathrm{kpc}$. The total trace back time is arbitrary, and it corresponds to an average age of the star forming regions in the solar neighbourhood. Many of our sources can live for much longer ages that 10 Myr [2], therefore they might come from a very different location than the one derived with a 10 Myr trace back. Another issue is that many of our sources are not traced back to star forming regions within 10 Myr. These problems are further discussed in Section 5.5.

To take into account errors on the measured quantities, we draw $N = 1000$ Monte Carlo (MC) realisations of each stars distance, proper motions, and radial velocity. Fig. 5.6 shows the distribution of the $(X, Y, Z)_{50} - (X, Y, Z)_{16}$ at $t = -10$ Myr. The distribution $(X, Y, Z)_{84} - (X, Y, Z)_{50}$ is similar. The typical error on the final position of each star after a trace back time of 10 Myr are large, with medians of $123, 89$, and $38\,\mathrm{pc}$ in X, Y, and Z respectively.

[2]For example, a B0.5V type star main sequence lifetime is around 11 Myr, a B5V type star main sequence lifetime is around 220 Myr, and a B9V type star main sequence lifetime is 700-800 Myr

5.4 Results

Fig. 5.7 shows the trajectories of 225 OB-type stars with measured radial velocity, colour-coded by the distance from the Sun at each trace back time. The total integration time is 10 Myr, however in the figure only the first 2 Myr are shown to avoid crowding. The current source positions are marked with a black cross. Of the 225 O and B-type candidate runaway stars with measured radial velocities, 115 (51 % of the sample) have distances smaller than 1 kpc when they enter or cross the plane for more than the 50% of the Monte Carlo simulations. The sources with ejection locations further than 1 kpc might have been ejected from clusters or star forming regions outside the solar neighbourhood.

We now focus on the candidates in two regions, Orion and Scorpius-Centaurus. The runaway star candidates in the Orion region are listed in Table 5.1. Their trajectory is shown in Fig. 5.8. The first two entries in the table (53 Ari and HD 43112) were recognised as runaway by Blaauw (1961) and Hoogerwerf et al. (2001). The origin of 53 Ari is not certain. It could have been ejected by one of the clusters in the Orion region (see Zari et al. 2019) or by a supernova explosion. HD 43112 (HIP 29678) is a B1V star likely ejected from the λ Ori cluster, together with HIP 22061 (which is not in our sample, see Table 5.3) as found by **?**. The other eight candidates in Table 5.1 have distances consistent with Orion, however further analysis is required to determine whether they have been ejected as a result of a supernova explosion or dynamical interactions within a cluster in the region. The trajectories of *Gaia* DR2 301...392 and *Gaia* DR2 320...656 seem to cross at $l, b \approx (195°, -8°)$ (see Fig. 5.8), however the distance from the Sun at which the orbits cross is $< 100\,\mathrm{pc}$, and, most importantly, the closest approach between the orbits occurs at different trace back times (between 7 and 8 Myr and between 6 and 7 Myr). This is therefore likely to be a chance alignment between the orbits projected in the sky, and the stars might have been ejected in the surrounding of the Orion nebula cluster or in the Belt region. The known Orion runaways AE Aur and μ Col are not in our candidate runaway list. AE Aur is not in the `StarHorse` catalogue (see Section 2), while μ Col is in `StarHorse` but it is removed by the conditions on the flags (in particular the *large distance flag* $= 1$, see Table 5.3). Since both of them are in the *Gaia* catalogue however, we confirmed that they are indeed coming from the Orion Nebula Cluster.

In Sco-Cen we noticed that *Gaia* DR2 349...472 and *Gaia* DR2 589...640 seem to come from the same point in the sky (their properties are reported in Table 5.2). By performing Monte Carlo simulations we found that both stars originate from Upper Centaurus Lupus (a sub-group of Sco-Cen, gray box in Fig. 5.9). The distances of the stars are consistent with the distance to the association (de Zeeuw et al. 1999), and the travel times are comparable (colour map in Fig. 5.9, right).

The known runaway ζ Oph (**?**Hoogerwerf et al. 2001), which was found to be ejected from a supernova explosion in the Upper Scorpius (US) sub-group of Sco-Cen, is not included in the `StarHorse` catalogue. Similarly to μ Col and AE Aur, we confirmed that it can be traced back to US by using *Gaia* DR2 astrometry.

The analysis of the orbits of the other runaway star candidates is currently on-going.

Table 5.1: *Gaia* `source_id`, Simbad identifiers, spectral types, observed radial velocities, and total peculiar velocities of the runaway sources whose trajectories cross the Orion region.

Gaia `source_id`	Name	Spectral type	v_r [km s^{-1}]	v_{tot} [km s^{-1}]
5885071133748761 6	53 Ari	B1.5V	21.7 ± 1.5	49.2
3344576352924411136	HD 43112	B1V	36.9 ± 0.7	71.7
3332953896541347200	HD 36824	B3V	17 ± 3.5	23.3
3015379032512681856	HD 37492	B8III	52 ± 1.5	36.9
3017367396223983616	HD 37061	O9V	67 ± 1	50.2
3223150304544227072	HD 38528	B9/9.5IV	65 ± 16.9	47.7
3012264940704649984	HD 38185	B8Ib/II	94 ± 6.9	78.1
3016120962343387392	HD 37889	B3II/III	52.6 ± 6	35.5
3209067866991398656	HD 36120	B8V	69.9 ± 4	51.8
3016713083716619520	HD 36487	B6IV	183.5 ± 39.4	166.7

Table 5.2: *Gaia* `source_id`, Simbad identifiers, spectral types, observed radial velocities, and total peculiar velocities of the runaway sources in the Sco-Cen region.

Gaia `source_id`	Name	Spectral type	v_r [km s^{-1}]	v_{tot} [km s^{-1}]
3498480561739049472	HD 111226	B8V	49 ± 7.4	65.6
5895765142704352640	V* V716 Cen	B5V	66 ± 10	76

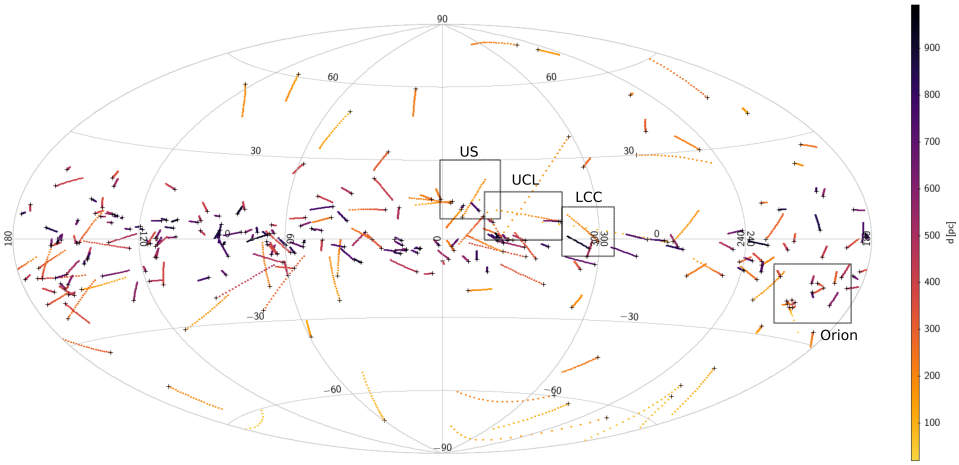

Figure 5.7: Trajectories of the OB-type runaway star candidates with measured radial velocities projected in the sky. The orbits are calculated for 2 Myr. The crosses represent the current position of the sources. The colour map represents the distance of the sources at each time step. The grey boxes represent the approximate locations of the regions analysed in more detail in Section 5.4. Upper Scorpius (US), Upper Centaurus Lupus (UCL), and Lower Centaurus Crux (LCC) are the sub-groups of the Scorpius-Centaurus association (Sco-Cen).

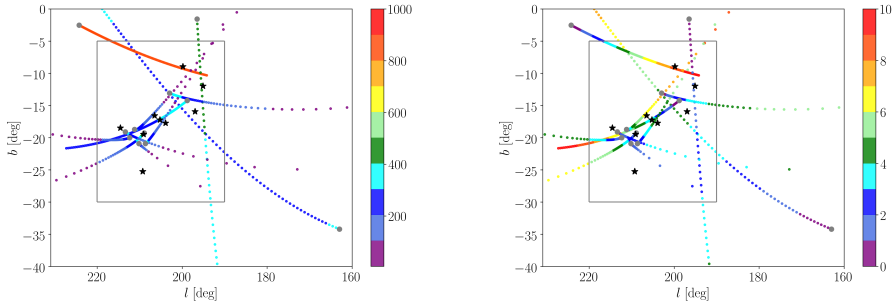

Figure 5.8: Trajectories of the OB-type runaway star candidates in the Orion region, colour-coded according to their distance (in parsec, left) and trace-back time (in Myr, right). The current source positions are shown by the gray dots. The black stars show the Orion constellation, and the grey box draws the boundaries of the complex (see Zari et al. 2017, 2019).

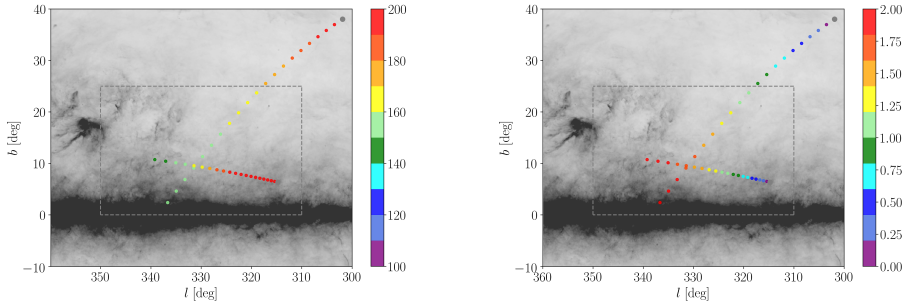

Figure 5.9: Same as Fig. 5.8 but for the two candidate runaway stars in Upper Centaurus Lupus. The background image shows dust extinction from the Planck satellite. The box corresponds to the boundaries of the Upper Centaurus Lupus region.

5.5 Discussion

In this Section we compare our runaway star candidates with other catalogues, in particular Hoogerwerf et al. (2001), Maíz Apellániz & Weiler (2018), and Tetzlaff et al. (2011), and with the results of the simulations by Renzo et al. (2019b) and Schoettler et al. (2019). Finally we discuss the completeness of our catalogue.

5.5.1 Comparisons with other runaway stars catalogues

Out of the 56 stars in Hoogerwerf et al. (2001), 55 are in the *Gaia* catalogue; 31 sources are left when cross-matching with the `StarHorse` catalogue, cleaned with the conditions `sh_outflag = "00000"` and `sh_gaiaflag = "000"`; 29 sources are left when applying the conditions in Eq. 5.1. Finally 20 stars are classified as runaways using the conditions $\Delta > 3$ or $v_{tot} > 30\,\mathrm{km\,s^{-1}}$. A summary of the comparison between our catalogue and Hoogerwerf et al. (2001) runaway star list is given in Table 5.3. As mentioned in Section 5.4, some of the known runaways are not included in the `StarHorse` catalogue (likely because of convergence problems), or are removed by one of the flags (see Section 5.2) or by the photometric criteria of Eq. 5.1.

We do not have any of the Maíz Apellániz & Weiler (2018) sources in our selection, mainly because of distance: indeed only 10 of their sources are within 1 kpc, 7 remain after we apply the StarHorse quality flags, and only 1 is left after applying Eq. 5.1. This source is not selected by the condition $\Delta > 3$. Some of the sources selected as runaway star candidates by Maíz Apellániz & Weiler (2018) show evidence of bow-shocks, which we do not find for any of the sources in our sample. This could depend on the fact that most of our stars are of spectral type B, and they might not have winds that are strong enough to produce bow shocks or that the medium in which they are located is not dense enough for the bow shock to be created: this is the case for stars at high galactic latitudes.

Tetzlaff et al. (2011) provide a catalogue of 2547 runaway stars of all spectral types (of which 835 are classified as O and B-type stars); 83 of our candidate runaway stars are in common with this sub-set. Tetzlaff et al. (2011) select runaway stars by using their complete kinematics when available, and tangential velocities only for sources without measured radial velocities.The large discrepancy in numbers is due to the same reasons why some of the runaway stars in Hoogerwerf et al. (2001) are not in our sample: some of them are not reported in the `StarHorse` catalogue, others do not pass the quality flags, others are left out as they do not comply with Eq. 5.1.

5.5.2 Comparison with simulations

In their simulations, Renzo et al. (2019b) study the evolution of massive binary systems to predict the peculiar velocities that stars obtain when their companion collapses and disrupts the system. In particular they investigate which physical processes leave a clear imprint and may therefore be constrained observationally. On of their main results is that the fraction of O-type runaway stars is at best of a few percent: this is however in tension with the observational result that 10-20% of the O-type stars are runaways. Our initial sample contains only 40 confirmed O-type stars, and

only four of them are selected as candidate runaways, therefore we can hardly draw any conclusion, without any further analysis of our candidates.

By performing N-body simulations of young stellar clusters, which do not include stellar evolution or primordial binaries, Schoettler et al. (2019) suggest that dynamical interactions during the early evolution of the clusters can produce runaway and walkaway stars. However, the runaways stars ejected in these simulations do not exceed masses of $0.5\mathrm{M}_{\odot}$. This result, together with the fact that the classical runaway production mechanisms may include also low-mass stars, imply that runaway and walkaway stars should be searched among all spectral types, and not only early type stars. For such studies however, it is necessary to focus on single star forming regions and their neighbourhood, and most importantly to be able to determine accurate ages for large samples.

5.5.3 Completeness

The first cut that might limit the completeness of our sample is the fact that we select stars nominally closer than 1 kpc ($\varpi > 1\,\mathrm{mas}$). By doing so, we do not consider the error on the parallax measurement, therefore we might be excluding stars with a measured parallax smaller than 1 mas, that are however compatible with being closer than 1 kpc.
As mentioned above, the `StarHorse` catalogue does not contain all the sources in *Gaia* DR2, but those that have converged. This is one of the main reasons for the very low number of sources in common with Tetzlaff et al. (2011). We also lose sources when selecting our sample by applying the *Gaia* and `StarHorse` quality flags. For instance, we might be loosing very bright sources by applying the condition $RUWE < 1.4$ (see Section 2).
In Section 5.3.1 we noticed that many sources with total peculiar velocity higher than $30\,\mathrm{km\,s^{-1}}$ were not selected as candidate runaway stars based only on their peculiar tangential velocity. Literature radial velocities are available only for 4352 stars, of which 340 ($\approx 8\%$) were not classified as runaway candidates based on their tangential velocity. If we assume this fraction to stay the same when considering the entire sample, we would be missing around a thousand runaway candidates from our selection (the total number of sources $\times$ 0.08 - 340). By adding these stars to our list, the fraction of runaways in our sample would be around 12-13%.

5.6 Conclusions

We use the `StarHorse` catalogue to search for early-type runaway stars in *Gaia* DR2. We identify O-, B-, and early A-type stars within 1 kpc from the Sun by performing a photometric selection in the $M_{G,0}$ vs. $(G_{\mathrm{BP}} - G_{\mathrm{RP}})_0$ colour-magnitude diagram, after correcting for extinction and reddening. The selection of candidate runaway stars is performed in two steps. We study the tangential velocity distribution of the early type stars, and we select as candidate runaway sources those whose tangential velocity is significantly different than the average tangential velocity at the same longitude angle. After cross-matching with radial velocity catalogues, we include in the candidate runaway source list also the stars whose total peculiar velocity is larger than

$30\,\mathrm{km\,s^{-1}}$. This is because stars with high radial velocity but tangential velocities comparable with those of field stars are not selected by using only tangential velocities. We integrate back in time the orbits of our candidate stars and we find that all of them are coming from the disc, although around half of our sample was probably originated at distances larger than 1 kpc. We study in more detail the runaway candidates in the Orion and Scorpius-Centaurus star forming regions, leaving to further studies a detailed analysis of all our candidate runaway stars. We compare our findings with previous studies, in particular Hoogerwerf et al. (2001), Maíz Apellániz & Weiler (2018), and Tetzlaff et al. (2011), and we discuss the (in)completeness of our sample. Future surveys (such as SDSS-V, WEAVE, 4MOST, and *Gaia* DR3) and targeted proposals for the brightest stars will increase the number of radial velocities available for the community, and will greatly improve the completeness of our sample.

Acknowledgements We thank F. Anders, A. Khalatyan, and C. Chiappini for making the `StarHorse` catalogue available in advance of publication, and D. Boubert for interesting discussions.
This work has made use of data from the European Space Agency (ESA) mission *Gaia* (`https://www.cosmos.esa.int/gaia`), processed by the *Gaia* Data Processing and Analysis Consortium (DPAC; `https://www.cosmos.esa.int/web/gaia/dpac/consortium`). Funding for the DPAC has been provided by national institutions, in particular the institutions participating in the *Gaia* Multilateral Agreement.

5.A Hoogerwerf et al. (2001) runaways in *Gaia* and `StarHorse`

Table 5.3: Hoogerwerf et al. (2001) Table 1 sources in *Gaia* DR2; ζ Puppis is not included because it is not in the *Gaia* DR2 catalogue. The ✓symbol indicates that a condtion is satisfied. The X symbol signifies that a condition is not satisfied, and therefore the star is excluded in the following columns (- symbol).

Gaia DR2 `source_id`	HIP ID	d < 1 kpc	`StarHorse`	`StarHorse` flags	$(G_{BP} - G_{RP})_0 \leqslant 0.5$ & $M_{G,0} \leqslant 0$	runaway selected
3904419434422220800	HIP 3478	✓	✓	✓	✓	✓
2890122152481960576	HIP 28756	✓	✓	✓	✓	✓
5625488726258364544	HIP 43158	X	-	-	-	-
3959631234670040704	HIP 61602	✓	X	-	-	-
4155626054317058048	HIP 91599	X	-	-	-	-
2083681294654108672	HIP 101350	✓	✓	✓	✓	✓
375010813139050368	HIP 3881	✓	✓	✓	✓	X
3344576352924411136	HIP 29678	✓	✓	✓	✓	✓
1132056347324894592	HIP 45563	X	-	-	-	-
5855802671032914944	HIP 62322	✓	X	-	-	-
6631708338599353856	HIP 92609	✓	X	-	-	-
2196984971452315392	HIP 102274	X	-	-	-	-
4718219005712946432	HIP 9549	✓	✓	✓	X	-
2891652569588715392	HIP 30143	✓	✓	X	-	-
5195896888895916288	HIP 46928	✓	✓	✓	✓	✓
6070376179105170048	HIP 66524	✓	✓	✓	✓	✓
6639975875765813888	HIP 94899	✓	✓	✓	✓	✓
6477764130748015488	HIP 103206	✓	✓	✓	✓	X
455030486274102272	HIP 10849	✓	✓	✓	✓	✓
3028075299444718080	HIP 35951	✓	✓	✓	✓	✓
5312887640522116992	HIP 46950	✓	✓	✓	✓	-
5895765142704352640	HIP 69491	✓	✓	✓	✓	✓
2049168552364523520	HIP 94934	✓	✓	✓	✓	✓
1963714268134133120	HIP 105811	X	-	-	-	-
58850711337487616	HIP 14514	✓	✓	✓	✓	✓
5611882304229988864	HIP 36246	✓	✓	✓	✓	X

5242303495131015808	HIP 48715	✗	-	-	-	-
6099307559838681216	HIP 70574	✓	✓	✓	✓	✓
2017735817073815680	HIP 95818	✓	✓	✓	✓	✓
1849597571190605952	HIP 106620	✗	-	-	-	-
2193759000051742 72	HIP 18614	✓	✓	✓	✓	✓
5537733610870346880	HIP 38455	✓	✓	✓	✓	✗
5660602557795903616	HIP 48943	✓	✗	-	-	-
5794330865689870592	HIP 76013	✓	✓	✗	-	-
2024645246873799040	HIP 96115	✓	✗	-	-	-
2199904449710846720	HIP 109556	✓	✓	✓	✓	✓
5511780021165932 80	HIP 20330	✓	✓	✗	-	-
5518235833732209536	HIP 38518	✓	✓	✗	-	-
5258611382897321088	HIP 49934	✓	✗	-	-	-
4337352305315545088	HIP 81377	✓	✗	-	-	-
2086465429887466368	HIP 97774	✗	-	-	-	-
3230156087694893952	HIP 22061	✓	✓	✓	✗	-
5352159374060797696	HIP 52161	✓	✓	✓	✓	✗
5927377029712024576	HIP 82171	✓	✓	✓	✓	✓
2086460069767734656	HIP 97845	✗	-	-	-	-
1820715707157130 24	HIP 24575	✓	✗	-	-	-
5547952884262112256	HIP 40341	✓	✓	✓	✓	✓
5333141671190375040	HIP 57669	✓	✓	✓	✓	✗
5936759471698278272	HIP 82868	✓	✗	-	-	-
2249990571599168512	HIP 99435	✓	✓	✓	✓	✓
2901155648586891648	HIP 27204	✓	✓	✗	-	-
5321174487856385664	HIP 42038	✓	✓	✓	✓	✗
6151098715037383552	HIP 59607	✓	✓	✓	✓	✓
4168881422863453568	HIP 86768	✓	✓	✓	✓	✗
2062426085622944256	HIP 99580	✗	-	-	-	-